Applied Energy 107 (2013) 281–296

Contents lists available at SciVerse ScienceDirect

Applied Energy

journal homepage: www.elsevier.com/locate/apenergy

Practical process design for in situ gasification of bitumen

Punitkumar R. Kapadia, Jingyi (Jacky) Wang, Michael S. Kallos, Ian D. Gates *

Department of Chemical and Petroleum Engineering, Schulich School of Engineering, University of Calgary, Calgary, Alberta, Canada T2N 1N4

HIGHLIGHTS

- In situ oil sands gasification processes produce energy in form of oil and syngas.
- Used comprehensive in situ bitumen gasification reaction system.
- In situ bitumen gasification model matched against field data.
- In situ gasification process is efficient, has lower emissions and water usage.

ARTICLE INFO

Article history:
Received 31 August 2012
Received in revised form 31 January 2013
Accepted 13 February 2013

Keywords:
Hydrogen
Gasification
Kinetics
Bitumen
Synthesis gas

ABSTRACT

The province of Alberta, Canada hosts an estimated 170 billion barrels of crude bitumen reserves in the Athabasca, Cold Lake and Peace River deposits. These reserves are commercially recovered through surface mining or in situ recovery methods. Most of the produced bitumen is converted in surface upgraders to synthetic crude oil (SCO), a 31–33°API oil product. Next, SCO is converted to transportation fuels, lubricants and petrochemicals in conventional refineries and petrochemical industries. In situ recovery or mining as well as bitumen upgrading and refining are energy intensive processes that generate huge volumes of acid gas, consume massive volumes of water, and are costly. Bitumen upgrading requires hydrogen, and currently most of it is produced by steam reforming of methane. Alternatively, hydrogen can be generated by in situ gasification of bitumen. In situ gasification of oil sands is potentially more energy efficient with reduced emission to atmosphere since acid gases are sequestered to some extent in the reservoir. Also, water usage is lowered and heavy metals and sulfur compounds in the bitumen tend to remain downhole since the main product is gas. The objective of this research was to understand and optimize hydrogen generation by in situ gasification from bitumen reservoirs. The central idea was to recover energy from the reservoir in the form of hydrogen and bitumen. In situ combustion has been attempted in the field, in a pilot run at Marguerite Lake. In this pilot, the produced gas contained up to 20 mole percent of hydrogen. In the current study, the Marguerite Lake Phase A main-pattern in situ combustion pilot was history-matched as a basis to understand a field-operated recovery process where in situ gasification reactions occur. Based on Marguerite Lake in situ combustion pilot observations, a new in situ bitumen gasification process, based on a Steam-Assisted Gravity Drainage (SAGD) well configuration, was designed and compared with conventional SAGD on the basis of energy investment, emission to atmosphere and water usage. The results show that the amount of energy produced per unit of energy invested for the in situ gasification process was greater than the steam alone recovery process with less than half the water usage. The cyclic injection of steam and oxygen as compared to steam injection alone can permit design of oil-alone to oil + syngas production processes.

1. Introduction

Global estimates of the volume of heavy oil and bitumen hosted in oil sands reservoirs is greater than six trillion barrels [1,2]. Western Canada alone contains over 1.7 trillion barrels of bitumen within oil sands reservoirs [3]. This volume of unconventional oil is the third largest globally behind the conventional oil resources of Saudi Arabia and unconventional resources of Venezuela [4]. The key difficulty associated with bitumen recovery from oil sands reservoirs is its high viscosity: at original conditions, it is typically hundreds of thousands to millions of centipoise. If the reservoir is shallow enough (typically <70 m), then the oil is recovered by surface mining. For deeper reservoirs, Cyclic Steam Stimulation (CSS) and Steam-Assisted Gravity Drainage (SAGD) are used. These methods inject steam into the oil sands formation to raise the temperature of the bitumen. At over about 200 °C, the viscosity of Athabasca bitumen drops to less than 10 cP (0.01 Pa s) which enables

* Corresponding author. Tel.: +1 403 220 5752; fax: +1 403 284 4852.
E-mail address: ian.gates@ucalgary.ca (I.D. Gates).

0306-2619/$ - see front matter © 2013 Elsevier Ltd. All rights reserved.
http://dx.doi.org/10.1016/j.apenergy.2013.02.035

it to be produced from the reservoir. In current practice, steam is generated by combustion of natural gas: as shown in Fig. 1, about 300 Sm^3 (assuming 8% heat losses in pipeline) of natural gas are required (for steam generation) per m^3 bitumen recovered for a cumulative steam-to-oil ratio (cSOR) of 2.5 m^3 per m^3. The corresponding amount of CO_2 emitted to the atmosphere as a result of this combustion is equal to about 560 kg per m^3 bitumen recovered.

On an energy basis, the energy invested by natural gas combustion in steam-based recovery processes (the energy intensity) such as SAGD and CSS, is equal to about 10 GJ per m^3 bitumen recovered at a steam-to-oil ratio (SOR) equal to about 4 m^3 per m^3. Given that the heating value of bitumen is ~43 GJ per m^3 [5], this means that in situ steam-based recovery processes are energy intensive and emit large quantities of CO_2 to atmosphere. If upgrading of bitumen and refining of synthetic crude oil is included, energy intensity and emission to atmosphere are even higher. During upgrading, roughly 180 Sm^3 of hydrogen are required per Sm^3 of synthetic crude oil (SCO) produced [6]. Given projections for increased oil sand development and consequent hydrogen consumption, there is a pressing need to develop more sustainable hydrogen production methods.

The combined motivation to (a) improve hydrogen generation and (b) increase bitumen recovery with lower emission to atmosphere and (c) lower water consumption, has driven us to study in situ gasification (ISG) of bitumen. In these types of the recovery processes, the energy vectors recovered consist of not only bitumen but also synthesis gas. The design of a process for in situ hydrogen generation by bitumen gasification requires construction of the reaction scheme together with associated kinetic parameters. Since bitumen, oxygen, and water coexist in the presence of heat during bitumen gasification, the reaction system should take into account pyrolysis (thermolysis, thermal cracking), aquathermolysis, gasification, and combustion (oxidation) reaction mechanisms.

Here, tuning of a proposed unified kinetic scheme, originally derived from matches to laboratory experiments [7–13], was carried out by history matching the Marguerite Lake in situ combustion (ISC) pilot conducted in the 1980s [14]. Because the Marguerite Lake pilot consistently produced hydrogen during CSS followed by ISC, it serves as not only a combustion pilot but also an ISG pilot and provides a data set from the field that can be used to tune kinetic parameters of the laboratory-derived reaction scheme to values appropriate for use in a field scale model. The pilot was conducted in the Clearwater Formation, an oil sands reservoir at a depth of 450 m with gross pay thickness equal to 34 m. In this formation, the porosity and permeability of reservoir were 30% and 1–3 D (9.8692×10^{-13} to 2.9608×10^{-12} m^2), respectively and the 12°API bitumen had viscosity, at original temperature and pressure, equal to about 100,000 cP (100 Pa s) [19]. As shown in Fig. 2, during the pilot test, Wells EX T2 and EX T3 were steam fractured and operated through several CSS cycles. Then, Well EX T4 was steam fractured and operated briefly for CSS before converted to air injection. During this combustion pilot, the produced gas consistently showed the presence of up to 20 mole percent of hydrogen in produced gas from Well EX T2 as a result of air and water co-injection in Well EX T4. The main pilot consisted of four five-spot patterns (Wells EX 1–EX 13) with an additional five infilled wells (Wells EX 21–EX 25). All main pilot wells were steam fractured and operated through six cycles of CSS. Also, air and water co-injection in Well EX 4 demonstrated consistent production of up to 20 mole percent of hydrogen in the produced gas from Well EX 5 [8,14–22].

We have previously developed and tested a comprehensive reaction scheme to simulate hydrogen generation from gasification of bitumen at laboratory-scale [12]. The research described here focuses on conceptual design and simulation of a field application of ISG to examine the potential to generate hydrogen directly from

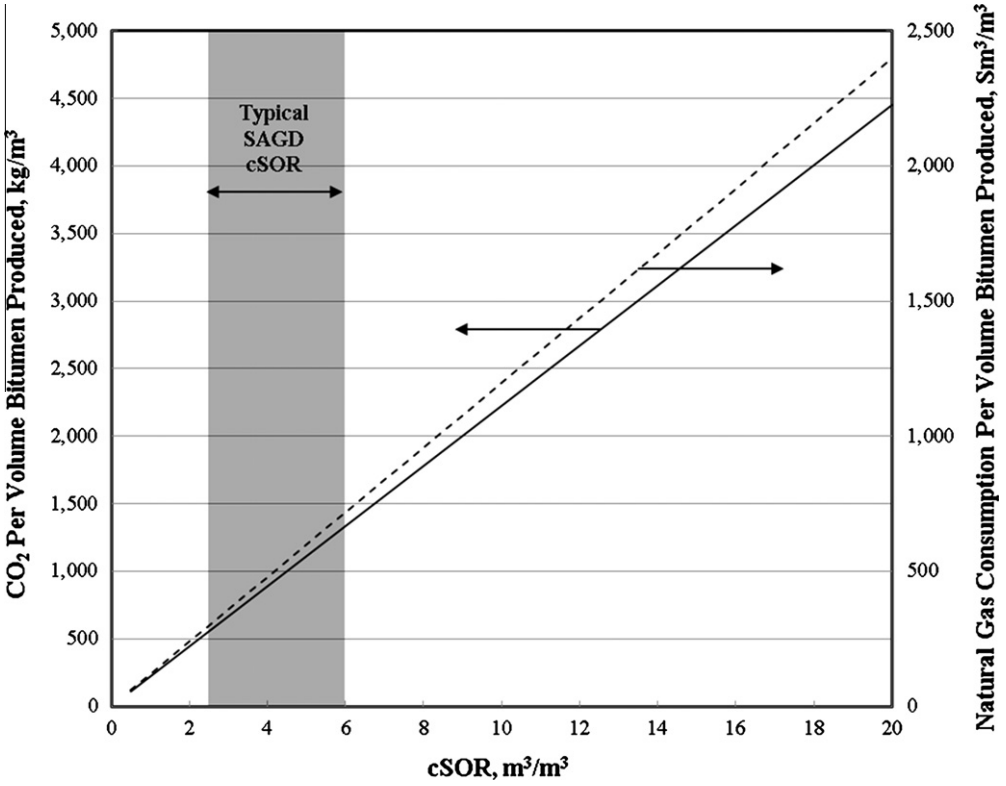

Fig. 1. Carbon dioxide emission and natural gas consumption per volume of bitumen produced versus cumulative steam oil ratio during typical SAGD operation for oil sands reservoir (assuming that thermal efficiency of steam generator is 75%). Typical cSOR for SAGD is 2.5–6 m^3 per m^3.

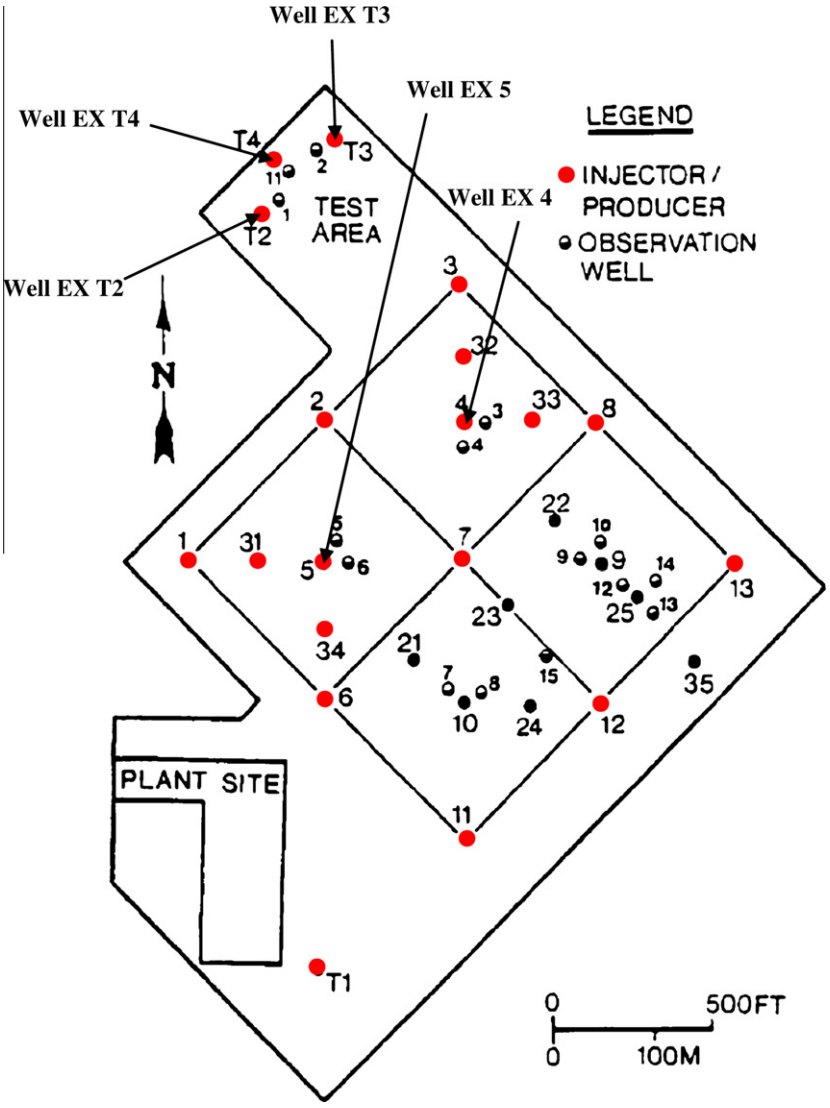

Fig. 2. Well configuration of the Marguerite Lake CSS + ISC pilot (modified from [20] with permission of Society of Petroleum Engineers).

the bitumen reservoir. During in situ hydrogen generation, there is also the potential for in situ upgrading of bitumen. ISG of bitumen has potential benefits over the traditional route of steam-based bitumen recovery from the reservoir, upgrading to synthetic crude oil, and then refining to transportation fuels. First, consumption of water is reduced or eliminated since less or no surface-generated steam is used and steam generation occurs in the reservoir itself. Second, because combustion occurs underground, a portion of the CO_2 and H_2S generated by the reactions will be sequestered within the reservoir, e.g. dissolved in oil or water or reacted with minerals. Third, much less natural gas is consumed on surface and thus emissions arising from steam generation are reduced. Fourth, thermal efficiency is increased since heat losses are reduced because heat is generated directly in the reservoir rather than on surface in a steam generator. Fifth, if in situ upgrading of bitumen occurs, then a value-added product is produced to surface.

2. Materials and methods

2.1. Bitumen gasification reaction scheme

ISG of bitumen constitutes a system of multiple complex reactions with different combinations of series and parallel reactions, displayed in Figs. 3 and 4, (described by [13,23]) and Fig. 5 [7–11,24]. The reaction system includes pyrolysis, aquathermolysis, low temperature oxidation (LTO), and high temperature oxidation (HTO) reactions. The reason oxidation reactions are included is because combustion is used to generate temperatures within the reservoir to enable gasification. In addition, there are also chemical interactions among the products of the reactions such as coke gasification, water gas shift, methanation, and methane, hydrogen, and other gas combustion reactions. The reaction system also involves pseudo-components to describe pyrolysis or combustion of asphaltenes, bitumen and vacuum residue [10,11,24–27].

As shown in Fig. 3, the pyrolysis reaction scheme consists of eight reactions and nine components. Here, in pyrolysis (largely occurs >300 °C), bitumen is represented by two pseudo-components: maltenes and asphaltenes. Given that the asphaltenes pseudo-component represents many individual components, when it reacts, it can be converted into different products through a parallel reaction system. High Molecular Weight Gas (HMWG) is another pseudo-component in the reaction scheme which represents all C_{2+} combustible gas. Collectively, Reactions 2–8 conserve the moles of all elements involved in the reactions.

Fig. 4 depicts the aquathermolysis reaction scheme used in the present study [23]. It consists of six reactions that represent the conversion of oil sand into non-condensable gases in the presence

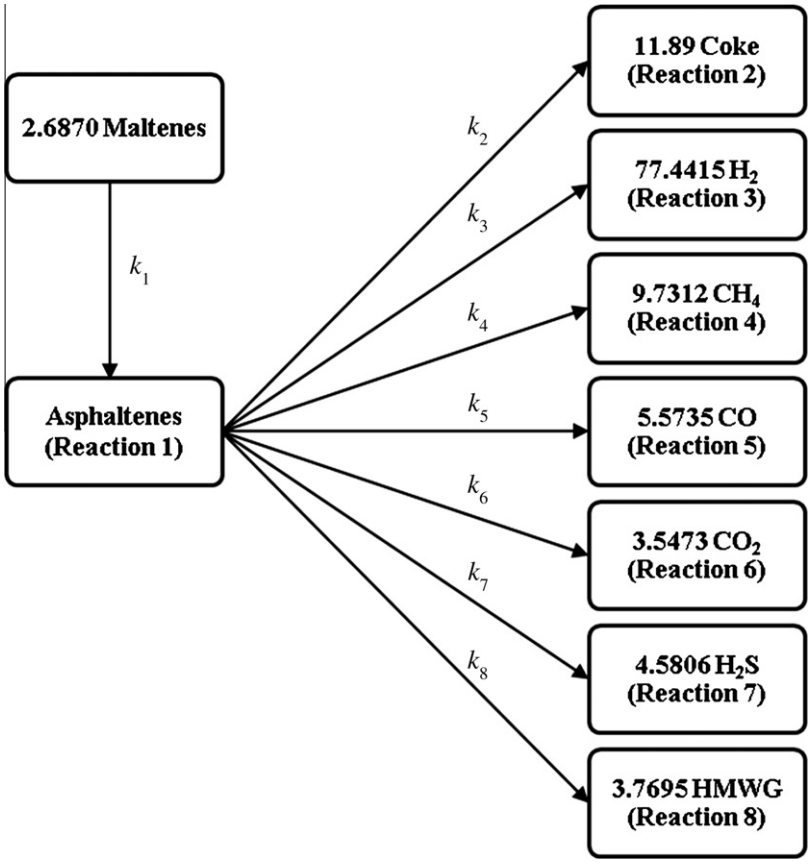

Fig. 3. Bitumen pyrolysis reaction scheme (reproduced from [13] with permission of Wiley). Bitumen consists of pseudo-components Maltenes and Asphaltenes.

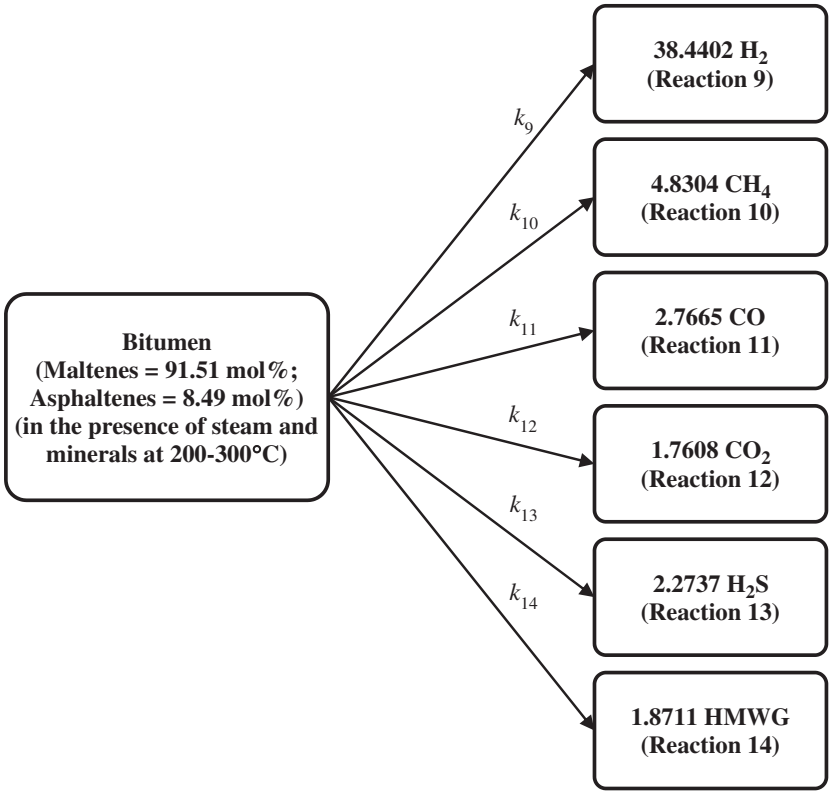

Fig. 4. Bitumen aquathermolysis reactions scheme (reproduced from [23] with permission of Elsevier).

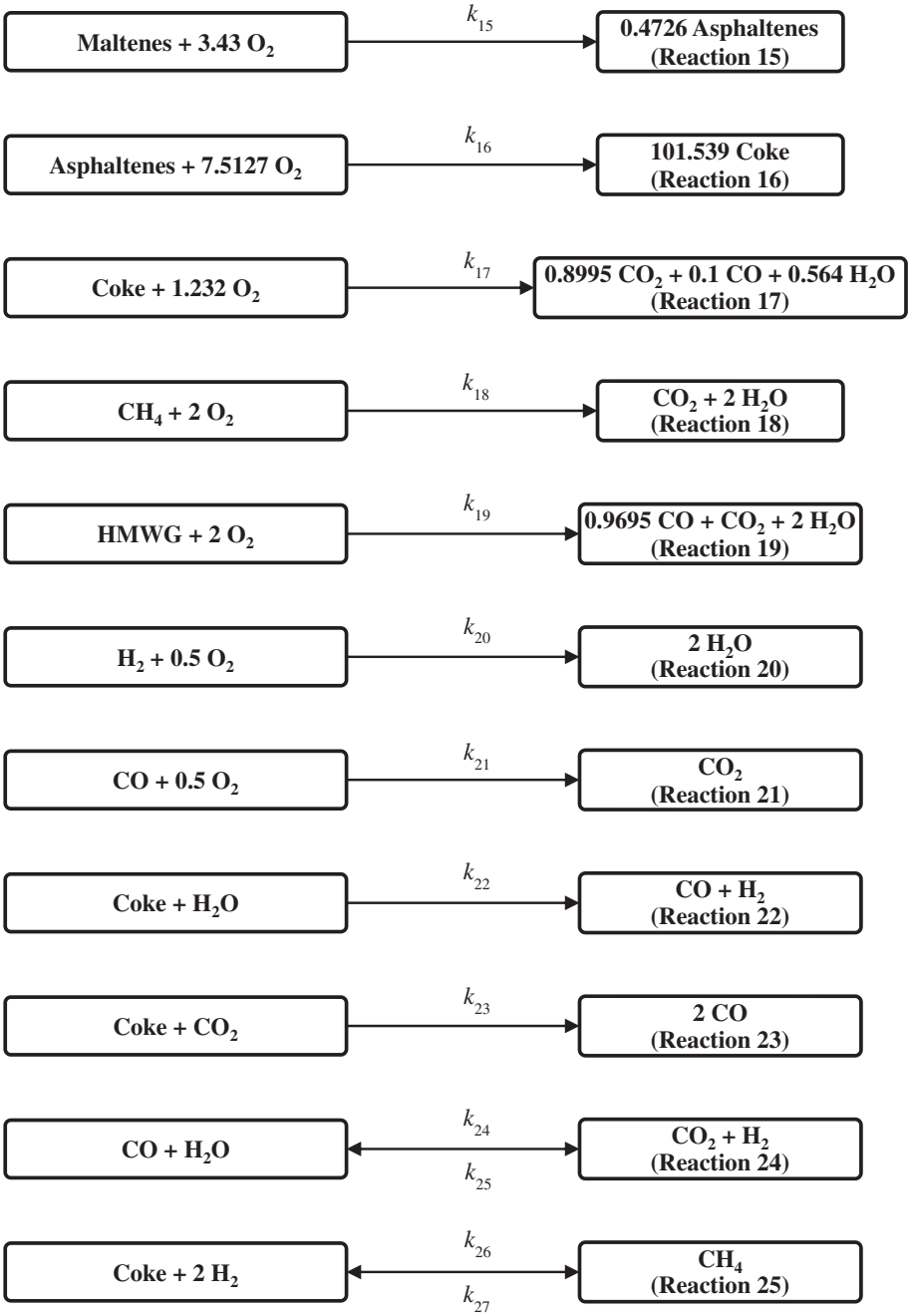

Fig. 5. Bitumen low temperature oxidation (Reactions 15 and 16) [10], high temperature oxidation (Reactions 17–21) [9,11,24], coke gasification (Reactions 22 and 23) [7,8], water gas shift (Reaction 24) [7,8], and methanation (Reaction 25) [7,8] reactions.

of steam as would be the case in an in situ steam-based recovery process such as SAGD. In aquathermolysis (typically <300 °C), bitumen is treated as a single component.

As described above, oxygen is injected into the oil reservoir to raise the temperature of the formation to values high enough to enable gasification. Fig. 5 depicts the reaction scheme for bitumen low temperature oxidation (LTO), coke high temperature oxidation (HTO) and other gas high temperature combustion, coke gasification, water–gas shift, and methanation reactions. The variation of which reactions dominate versus temperature is a result of kinetic parameters. LTO reactions are dominant in temperature range from 150 to 300 °C. HTO reactions basically contribute to most of the energy generated during gasification of bitumen. Coke gasification, water–gas shift, pyrolysis, and aquathermolysis reactions mainly generate hydrogen whereas methanation and hydrogen combustion reactions consume hydrogen. Table 1 describes the properties of components and pseudo-components used in the reaction system displayed in Figs. 3–5. The frequency factor and activation energy of Reactions 1–25 are listed in Table 2.

ISC takes place over two temperature and oxygen consumption ranges. For bitumen, LTO takes place between 150 and 300 °C where the oxygen consumption rates are relatively lower, whereas HTO occurs between 380 and 800 °C with higher oxygen consumption rates. Combustion experiments reveal that ahead of the combustion zone, the temperature of oil sand is increased as a result of heat conduction and because of the absence of oxygen, thermal cracking reactions convert maltenes to asphaltenes and asphaltenes to coke [10,28–31]. Where the oxygen concentration is low,

Table 1
List of components and pseudo-components and their properties [10,38].

Component	Molecular weight M_w, kg/gmol	Critical temperature T_C, °C	Critical pressure P_C, kPa
Maltenes	0.4067	618.85	1478
Asphaltenes	1.0928	903.85	792
Methane	0.01604	−82.55	4600
Hydrogen	0.002016	−239.96	3394
Carbon monoxide	0.02801	−140.25	3496
Carbon dioxide	0.04401	31.05	7376
Hydrogen sulfide	0.03408	100.4	9007
HMWG	0.04141	21.85	7176
H_2O	0.01802	373.85	22,107
Oxygen	0.032	−119.15	5046
Coke	0.01313	–	–

Table 2
The frequency factor and activation energy for Reactions 1–25.

Reaction	Refs.	Frequency factor A, day^{-1} except where noted	Activation energy E, J/gmol
1	[13]	1.174×10^{18}	2.358×10^{5}
2	[13]	3.110×10^{15}	1.897×10^{5}
3	[13]	2.227×10^{5}	9.963×10^{4}
4	[13]	2.565×10^{8}	1.122×10^{5}
5	[13]	6.360×10^{1}	4.892×10^{4}
6	[13]	1.874	2.313×10^{4}
7	[13]	3.385×10^{6}	9.721×10^{4}
8	[13]	6.172×10^{15}	2.013×10^{5}
9	[23]	3.000×10^{1}	8.123×10^{4}
10	[23]	6.800×10^{-2}	5.545×10^{4}
11	[23]	9.900×10^{-5}	1.168×10^{4}
12	[23]	3.700×10^{-5}	4.548×10^{3}
13	[23]	2.500×10^{-1}	5.471×10^{4}
14	[23]	3.100×10^{5}	1.162×10^{5}
15	[10]	$1.107 \times 10^{10}\ day^{-1}\ kPa^{-0.4246}$	8.673×10^{4}
16	[10]	$3.578 \times 10^{9}\ day^{-1}\ kPa^{-4.7627}$	1.856×10^{5}
17	[11,24]	$3.881\ day^{-1}\ kPa^{-1}$	8.205×10^{2}
18	[11,24]	$3.020 \times 10^{10}\ day^{-1}\ kPa^{-1}$	5.945×10^{4}
19	[11,24]	$1.311 \times 10^{8}\ day^{-1}\ kPa^{-1}$	2.662×10^{5}
20	[9]	$8.986 \times 10^{13}\ m^3\ kmol^{-1}\ day^{-1}$	1.255×10^{5}
21	[9]	$1.123 \times 10^{13}\ m^3\ kmol^{-1}\ day^{-1}$	1.255×10^{5}
22	[7,8]	2.117×10^{7}	9.200×10^{4}
23	[7,8]	2.592×10^{5}	5.300×10^{4}
24 (Forward)	[7,8]	5.573×10^{7}	1.490×10^{5}
24 (Reverse)	[7,8]	4.214×10^{9}	1.900×10^{5}
25 (Forward)	[7,8]	3.162×10^{4}	4.140×10^{4}
25 (Reverse)	[7,8]	7.113×10^{9}	1.163×10^{5}

LTO reactions dominate the process leading to formation of oxygenated oil compounds and coke. Where the oxygen concentration is high, HTO reactions dominate and coke produced by thermal cracking and LTO converts to carbon oxides. Beyond these oxidation zones, where the temperature is elevated to about >300 °C, thermal cracking reactions occur. The main products of thermal cracking are coke and non-condensable gases. The reaction zones anticipated in an ISG process heated by ISC are complex and interact over relatively small length scales and include not only combustion and thermal cracking zones but also aquathermolysis and gasification zones. For the design of hydrogen generation process, one key challenge is that the generated hydrogen and injected oxygen can react to form water. With respect to in situ process dynamics, since ISC is used to raise the temperature to enable gasification, for hydrogen production, implies that hydrogen generation reactions must occur outside of the combustion zone where there is no oxygen.

2.2. Reservoir simulation model for Marguerite Lake history match

As shown in Fig. 2, the combustion field pilot consists of injecting enriched air and water into Well EX 4. While this occurred, produced gas concentration profiles were measured in the produced gas from Well EX 5. The kinetic model proposed here was used to carry out the history match for Wells EX 4 and EX 5. As was done in the pilot, Wells EX 4 and EX 5 were switched to air injection after six cycles of CSS [8].

To history match gas generation from Well EX 5, an air injection (post CSS) submodel was extracted from four adjacent five-spot patterns as shown in Fig. 2. To be clear, the five-spot pattern consisted of four injection wells located at the corners of a square and a production well situated at the center of the square. Fig. 6 displays grid depth, permeability, porosity, and oil saturation distributions of the air injection (post CSS) submodel. During the air injection pilot, Well EX 4 was switched to an air injection well whereas Well EX 5 was switched to a production well. In the cross-well direction, there were 30 20-m gridblocks in the North-East direction whereas there were nine 20-m gridblocks in the North-West direction. There were 37 0.8-m long gridblocks in the downwell direction. The average horizontal permeability was 1836 mD ($1.8120 \times 10^{-12}\ m^2$) whereas the average porosity was equal to 27%. The oil column was 29 m thick with average oil saturation equal to 0.55. Table 3 lists the properties used in the reservoir simulation model. For the production well (Well EX 5), a total liquid control constraint, illustrated in Fig. 7, was applied to match field total liquid production rate data as obtained from AccuMap®

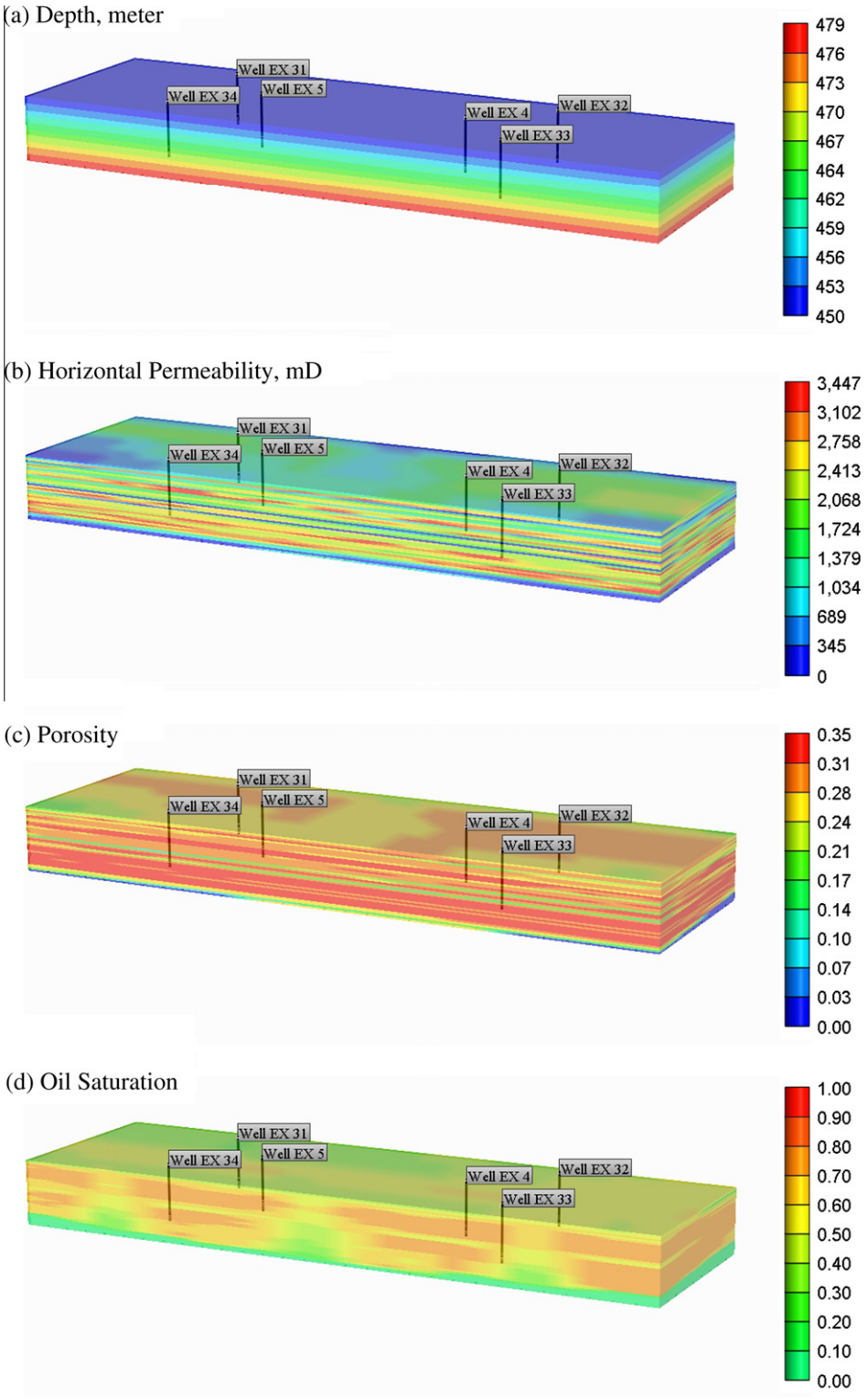

Fig. 6. Three-Dimensional views of reservoir properties (aspect ratio $z/x = 2$): (a) grid indicating the depth, in meters, (b) horizontal permeability, in mD, (c) porosity, and (d) oil saturation.

[32]. Similarly for the injection well (Well EX 4), the oxygen and water injection rates were imposed as per the field data [8], shown in Fig. 8.

Air injection was initiated in March 1983 into Well EX 4. Varying amounts of air were injected until late May after which pure nitrogen was injected for two weeks. Thereafter, air was again injected for about two weeks. After the air injection period, water injection occurred until the second week of August after which low rates of water were maintained until the second week of October when enriched air injection was resumed.

Table 3
Input data used in Marguerite Lake Phase A combustion pilot simulation model.

Parameter	Value		
Grid blocks	30 (I) × 9 (J) × 37 (K)		
Average horizontal permeability, mD	1836 (1.8120×10^{-12} m^2)		
Average vertical permeability, mD	982 (9.6916×10^{-13} m^2)		
Average oil saturation	0.55		
Average water saturation	0.38		
Original oil in place, m^3	1.1349×10^5		
Rock heat capacity, J/m^3 °C (also used for overburden and understrata)	2.600×10^6		
Rock thermal conductivity, J/m day °C (also used for overburden and understrata)	6.600×10^5		
Water phase thermal conductivity, J/m day °C	5.350×10^4		
Oil phase thermal conductivity, J/m day °C	1.150×10^4		
Gas phase thermal conductivity, J/m day °C	5.000×10^3		
	S_W	k_{rw}	k_{row}
Water-oil relative permeability curve (S_W = water saturation, volume fraction, k_{rw} = relative permeability of water phase k_{row} = relative permeability of oil phase with when water phase is present)	0.1500	0.0000	0.9920
	0.2000	0.0002	0.9790
	0.2500	0.0016	0.9500
	0.3000	0.0055	0.7200
	0.3500	0.0130	0.6000
	0.4000	0.0254	0.4700
	0.4500	0.0440	0.3500
	0.5000	0.0698	0.2400
	0.5500	0.1040	0.1650
	0.6000	0.1480	0.1100
	0.6500	0.2040	0.0700
	0.7000	0.2710	0.0400
	0.7500	0.3520	0.0150
	0.8000	0.4470	0.0000
	0.8500	0.5590	0.0000
	0.9000	0.6870	0.0000
	0.9500	0.8340	0.0000
	1.0000	1.0000	0.0000
	S_L	k_{rg}	k_{rog}
Gas–liquid relative permeability curve (S_L = liquid saturation (water + oil), volume fraction, k_{rg} = relative permeability of gas k_{rog} = relative permeability of liquid (water + oil) phase when gas phase is present)	0.1500	1.0000	0.0000
	0.2000	0.9500	0.0002
	0.2500	0.8400	0.0016
	0.3000	0.7200	0.0055
	0.3500	0.6000	0.0130
	0.4000	0.5030	0.0254
	0.4500	0.4284	0.0440
	0.5000	0.3598	0.0698
	0.5500	0.3069	0.1040
	0.6000	0.2659	0.1480
	0.6500	0.2214	0.2040
	0.7000	0.1781	0.2710
	0.7500	0.1408	0.3520
	0.8000	0.1095	0.4470
	0.8500	0.0770	0.5590
	0.9000	0.0481	0.6870
	0.9500	0.0241	0.8340
	1.0000	0.0000	0.9920

3. Results and discussion

For the history match of the field operation, kinetic parameters (as listed in Table 2), total liquid production rates (as displayed in Fig. 7), and enriched air and water injection rates (as displayed in Fig. 8) were kept unchanged. The reservoir simulation parameters that were tuned to match the field data were solution gas, extent of oxygen enrichment, and relative permeability curves. The simulations were carried out by using a commercial thermal reservoir simulator STARS™ [33].

Figs. 9–11 compare gas composition, and the cumulative gas and oil produced from Well EX 5 from the tuned reservoir simulation model with field data. The results reveal that the tuned model provides a reasonable representation of the field data. As shown in Fig. 9, when air injection was switched in March 1983 to Well EX 4 there was sudden drop in concentration of methane and slight drop in HMWG components produced from Well EX 5. Because of the onset of combustion, the concentrations of carbon oxides, hydrogen, and H_2S rose. The hydrogen and H_2S concentration profiles also showed good behavioral match after two weeks of nitrogen injection (Figs. 8 and 9). Fig. 10 presents a good match between simulation results and field data for cumulative gas production from Well EX 5. It can be seen that due to air injection in March 1983, there was a sudden rise in cumulative gas production from Well EX 5, which was very well predicted by the current reaction model. Fig. 11 shows a good match between simulation results and field data for cumulative oil production from Well EX 5 for beginning and end of air injection tests whereas there was a reasonable match obtained for the periods in between.

3.1. ISG process with SAGD well configuration

After field scale testing of the proposed reaction system for bitumen combustion, the predictions for an ISG process were carried out by predictive SAGD reservoir scale simulation of a typical oil sands reservoir wherein steam and oxygen were cyclically

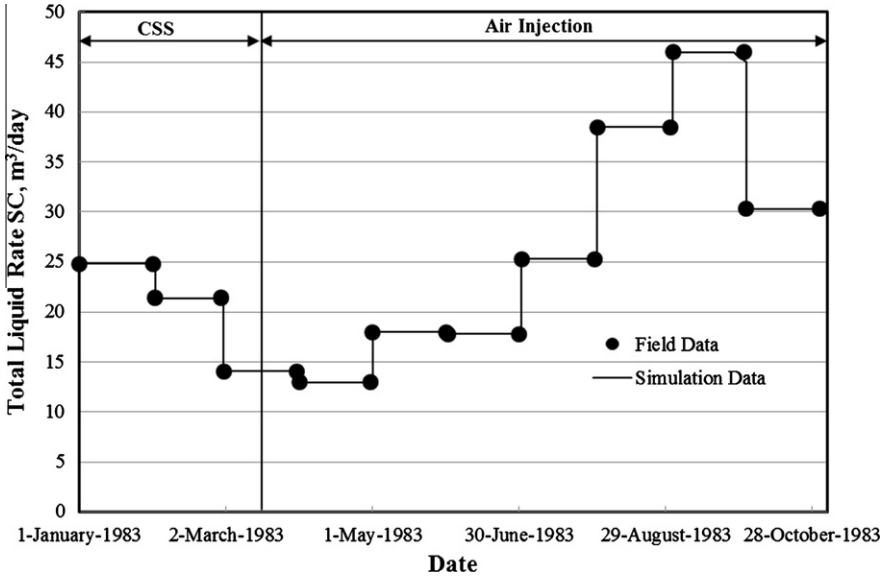

Fig. 7. Total liquid production rate – field data obtained from AccuMap® [32] – for Well EX 5 used as constraint during enriched air injection in Well Ex 4.

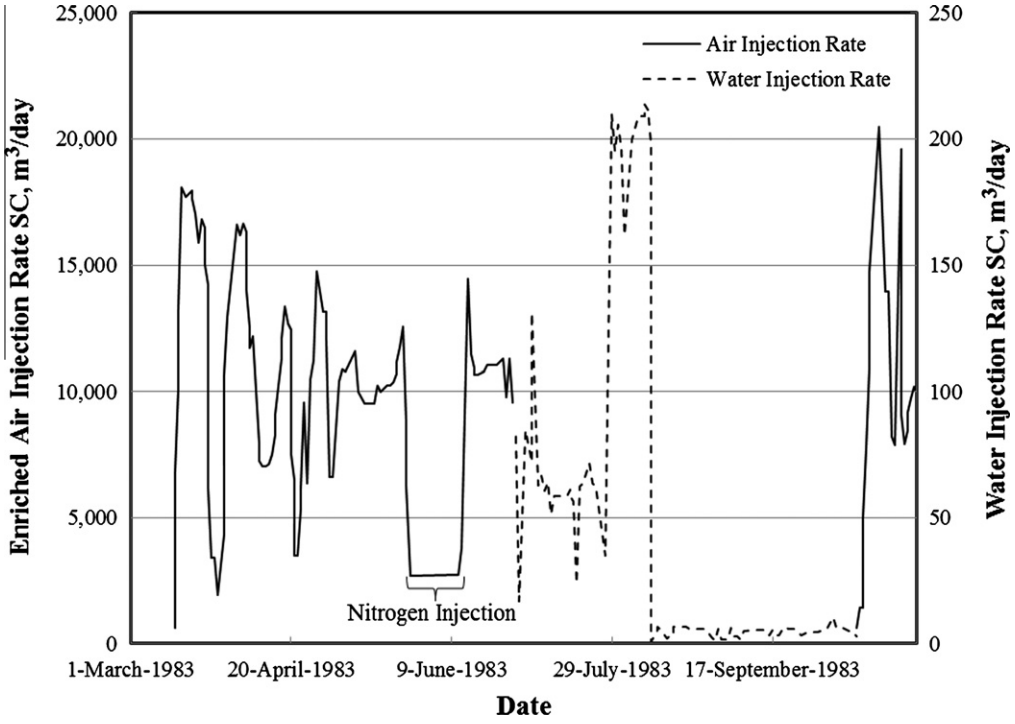

Fig. 8. Field data for enriched air (solid line) and water (dashed line) injection rates imposed for Well EX 4 (Reproduced from [8]).

injected into the upper well to study the amount of hydrogen generated from the lower well, i.e., the producer. The geological model had properties typical of an oil sands reservoir, as an exact geological model of this field was not available. As shown in Fig. 12 and Table 4, the model consisted of a symmetric two-dimensional model with homogeneous geology and fluid saturations. A SAGD wellpair configuration was used; the upper injection and lower production horizontal wells were located at the right side of the model. There were 58 0.8-m gridblocks in cross-well direction whereas there were 60 0.5-m grid-blocks in the vertical direction. The length of the wellpair was 750-m. The production well was positioned 6 m above the bottom of the reservoir whereas the injection well was located 5 m above the producer. Key reservoir properties are listed in Table 4. Prior to the beginning of injection, steam circulation was modeled by using temporary heaters in the locations of the injection and production wells for 90 days. To avoid build-up of pressure at the well locations, a temporary production well was placed in the model at the location of the injection well and both the temporary and lower production wells were operated with minimum bottom hole pressure set equal to the initial reservoir pressure at their depths. After the pre-heating period was done, the line heaters were turned off, the temporary

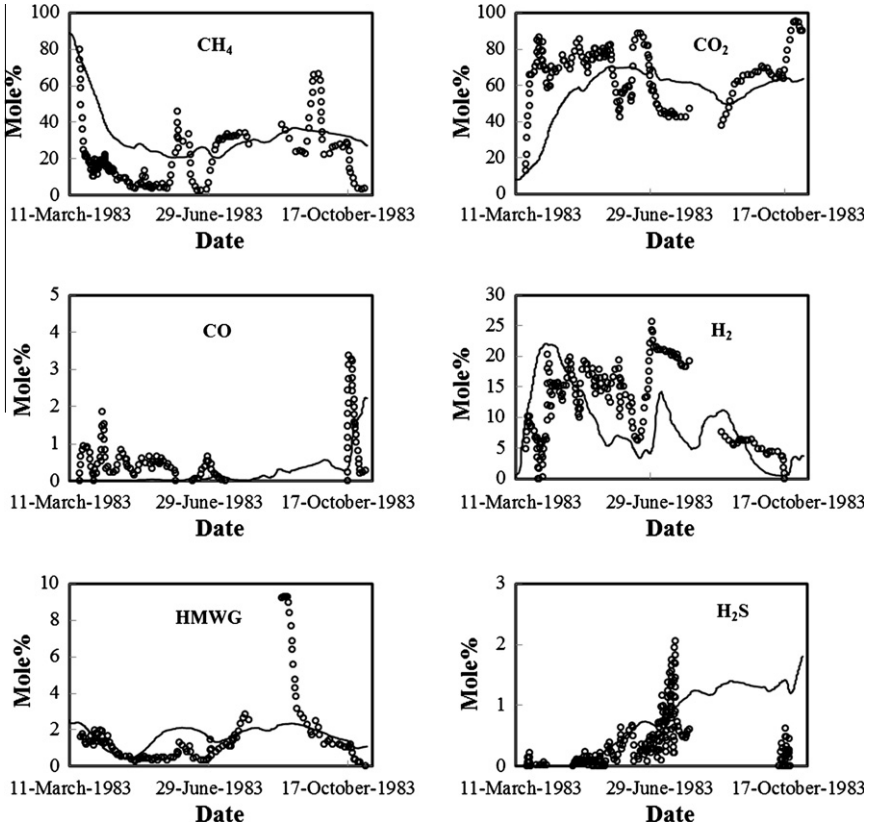

Fig. 9. Comparison between field data (empty circles, from [8]) and simulation results (solid line) for methane, carbon oxides, heavy molecular weight gas, hydrogen, and H_2S concentration profiles (nitrogen free basis) obtained from Well EX 5 during air and water injection in Well EX 4. Air injection begins from mid of May 1983.

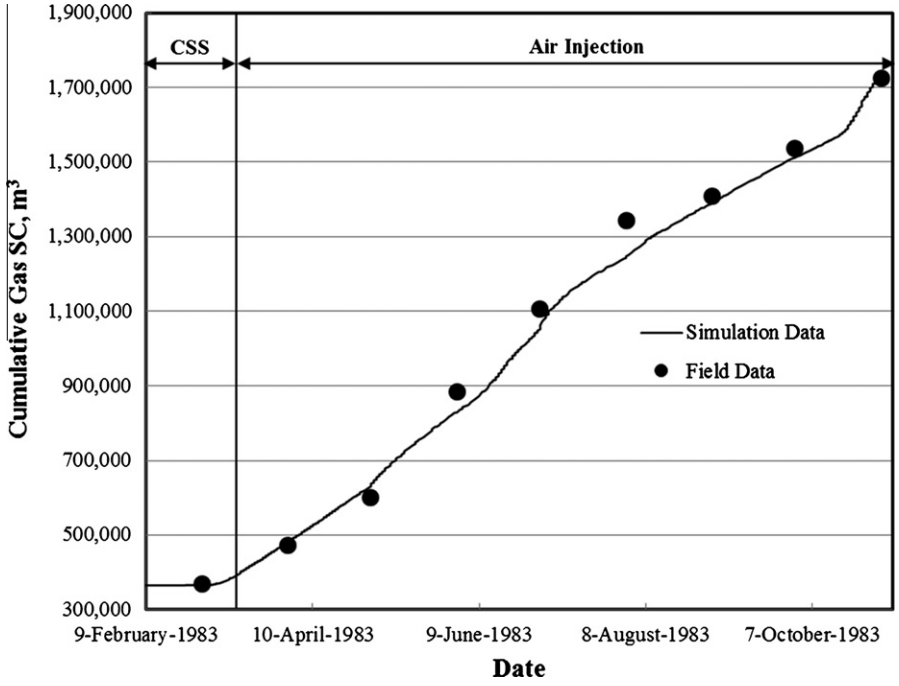

Fig. 10. Comparison between field data (dotted points) and simulation results (solid line) for cumulative gas production from Well EX 5 during air and water injection in Well EX 4.

production well in the location of the injection well was removed, and steam–oxygen injection phase was initiated into the top well. A SAGD case was also run without oxygen injection to compare its performance to the steam–oxygen process.

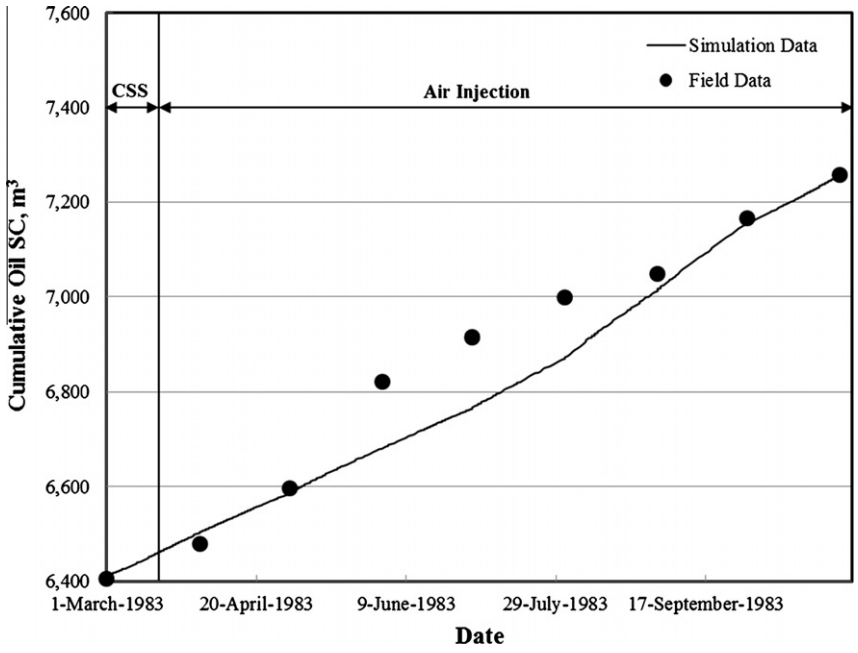

Fig. 11. Comparison between field data (dotted points) and simulation results (solid line) for cumulative oil production from Well EX 5 during air and water injection in Well EX 4.

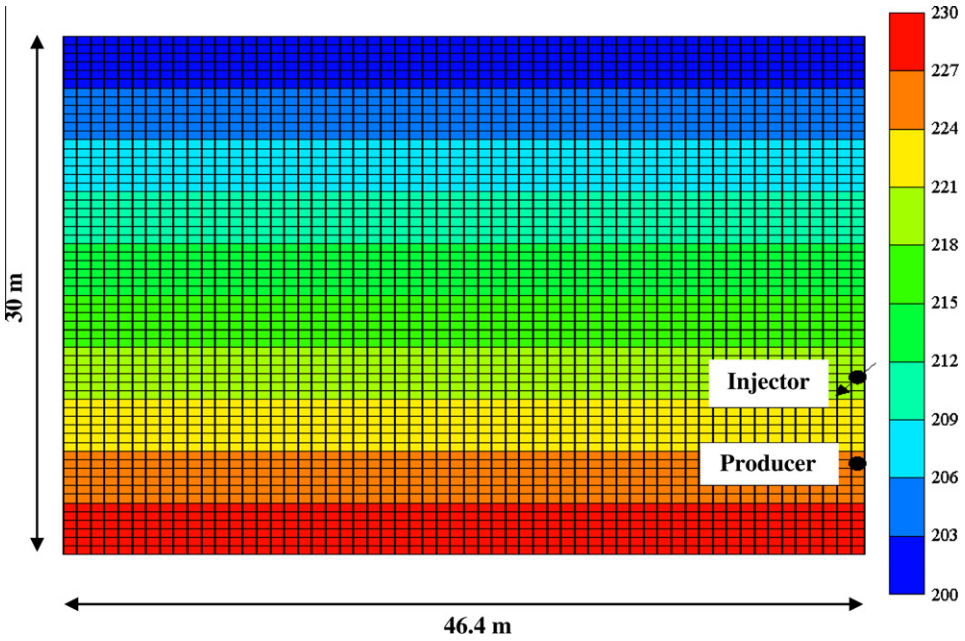

Fig. 12. Cross-sectional view of grid for two-dimensional model with SAGD-like well configuration. The color scale indicates the depth in meters from the surface. The model has a symmetry boundary with injector and producer located at the right side of the model.

Fig. 13 displays the cumulative steam for the SAGD and steam–oxygen ISG processes as well as the cumulative oxygen injected in the hybrid process. In the steam–oxygen hybrid process, each slug of steam (saturated steam at 200 °C with 95% steam quality) and subsequent slug of oxygen were injected for 90 days each. For the production well, steam-trap control was used by limiting the steam production rate to 1 m^3 CWE per day (CWE: Cold Water Equivalent) during the steam injection period whereas a minimum bottom hole pressure constraint was used during the oxygen injection period.

Fig. 14 displays the evolution of temperature at the end of each injection phase during steam–oxygen cyclic injection. The results reveal that during oxygen injection, the steam zone temperature reached high enough for combustion (>450 °C) and moved outwards from the injection well. Fig. 15 compares the cumulative oil and cumulative steam–oil ratio profiles for SAGD process (steam–oxygen injection) including chemical reactions with profiles obtained for the SAGD process (steam injection only, no chemical reactions occur). It is shown that cumulative oil production was lower and cumulative steam-to-oil ratio was higher for the

Table 4
Input data used for simulation model to predict generation of hydrogen during SAGD-air injection process.

Parameter	Value		
Grid blocks	58 (horizontal) × 60 (vertical)		
Horizontal permeability, mD	4000 (3.9477×10^{-12} m^2)		
Vertical permeability, mD	2000 (1.9738×10^{-12} m^2)		
Oil saturation	0.75		
Water saturation	0.25		
Initial reservoir temperature, °C	11		
Initial reservoir pressure, kPa	2,000		
Rock heat capacity, J/m^3 °C (also used for overburden and understrata)	2.600×10^6		
Rock thermal conductivity, J/m day °C (also used for overburden and understrata)	6.600×10^5		
Water phase thermal conductivity, J/m day °C	5.350×10^4		
Oil phase thermal conductivity, J/m day °C	1.150×10^4		
Gas phase thermal conductivity, J/m day °C	5.000×10^3		
	S_W	k_{rw}	k_{row}
Water–oil relative permeability curve (S_W = water saturation, volume fraction, k_{rw} = relative permeability of water phase k_{row} = relative permeability of oil phase with when water phase is present)	0.1500	0.0000	0.9920
	0.2000	0.0002	0.9790
	0.2500	0.0016	0.9500
	0.3000	0.0055	0.7200
	0.3500	0.0130	0.6000
	0.4000	0.0254	0.4700
	0.4500	0.0440	0.3500
	0.5000	0.0698	0.2400
	0.5500	0.1040	0.1650
	0.6000	0.1480	0.1100
	0.6500	0.2040	0.0700
	0.7000	0.2710	0.0400
	0.7500	0.3520	0.0150
	0.8000	0.4470	0.0000
	0.8500	0.5590	0.0000
	0.9000	0.6870	0.0000
	0.9500	0.8340	0.0000
	1.0000	1.0000	0.0000
	S_L	k_{rg}	k_{rog}
Gas–liquid relative permeability curve (S_L = liquid saturation (water + oil), volume fraction, k_{rg} = relative permeability of gas k_{rog} = relative permeability of liquid (water + oil) phase when gas phase is present)	0.1500	1.0000	0.0000
	0.2000	0.9500	0.0002
	0.2500	0.8400	0.0016
	0.3000	0.7200	0.0055
	0.3500	0.6000	0.0130
	0.4000	0.4700	0.0254
	0.4500	0.3500	0.0440
	0.5000	0.2400	0.0698
	0.5500	0.1650	0.1040
	0.6000	0.0930	0.1480
	0.6500	0.0750	0.2040
	0.7000	0.0450	0.2710
	0.7500	0.0270	0.3520
	0.8000	0.0200	0.4470
	0.8500	0.0100	0.5590
	0.9000	0.0050	0.6870
	0.9500	0.0000	0.8340
	1.0000	0.0000	0.9920

SAGD process with air and oxygen cyclic injection when compared to conventional SAGD process with steam injection only. This is because of the generation of product gases as shown in Figs. 3–5 during oxygen injection which reduced steam partial pressure and hence heat transfer rates to native bitumen.

Figs. 16 and 17 show the composition of the gas produced during cyclic injection of steam and oxygen. It can be seen that during first 90 days (the pre-heat period), since the temperature is comparatively lower, the produced gas was mainly solution gas (i.e., methane), and subsequently with the beginning of steam injection there was a slight increase in CO_2 and decrease in methane concentration. In general, during steam injection, the produced gas was composed of primarily of solution gas and gases produced due to aquathermolysis and pyrolysis and with more time, the extent of contribution from these reactions increased, because of higher steam chamber temperatures and volumes (shown in Fig. 14), resulting in an increase of these gas concentrations in produced gas during later cycles. Similarly during oxygen injection, the presence of higher concentrations of CO_2 implied that high temperature oxidation was occurring. At the beginning of the process, the hydrogen concentration ranged from 10 to 15 mole percent. In later cycles, it climbed to between 30 and 35 mole percent. In typical analysis, only the physical phenomena are examined but here, the steam chamber also behaves as a chemical reactor. Given that the chamber grows as the process evolves, this means that the reactor volume was not constant through the cycles. In the early stages of the process, during oxygen injection, the amount of coke deposited and steam chamber volumes were low. Coke deposition and the chamber volume increased in later cycles. Hence, with higher coke deposition and increased thermal cracking reactions during later cycles, the hydrogen concentration rose in the produced gas. Aquathermolysis, pyrolysis, and combustion reactions were main contributors for all gas components. The majority of CO_2 was generated from combustion. Similarly, the solution gas

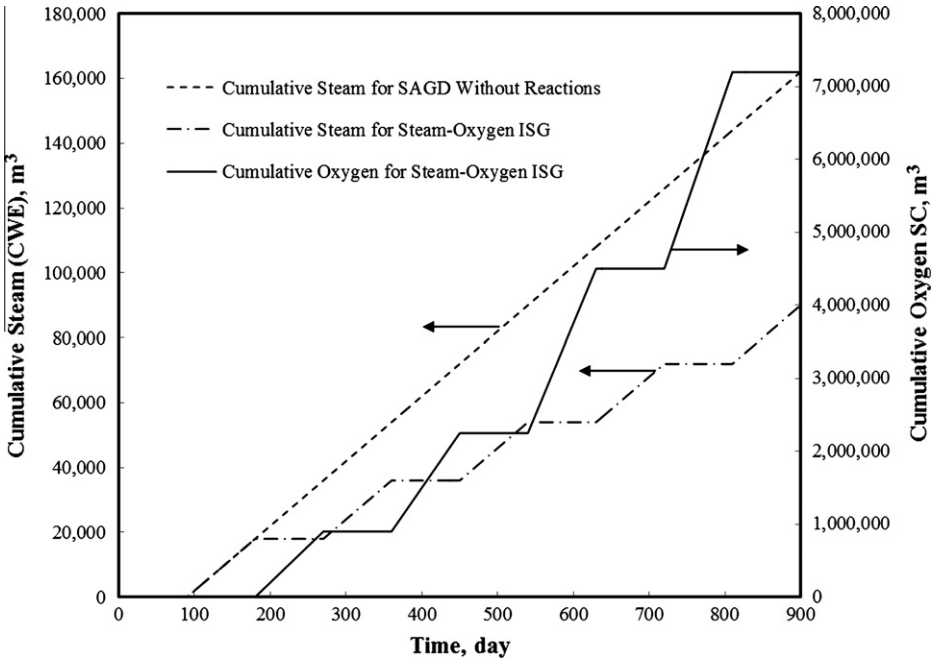

Fig. 13. Cumulative steam (expressed here as cold water equivalent (CWE)) and oxygen injection volumes (at standard conditions) versus time for SAGD process with (steam–oxygen injection) and without (steam injection) reactions. ISG in plot legend stands for In Situ Gasification.

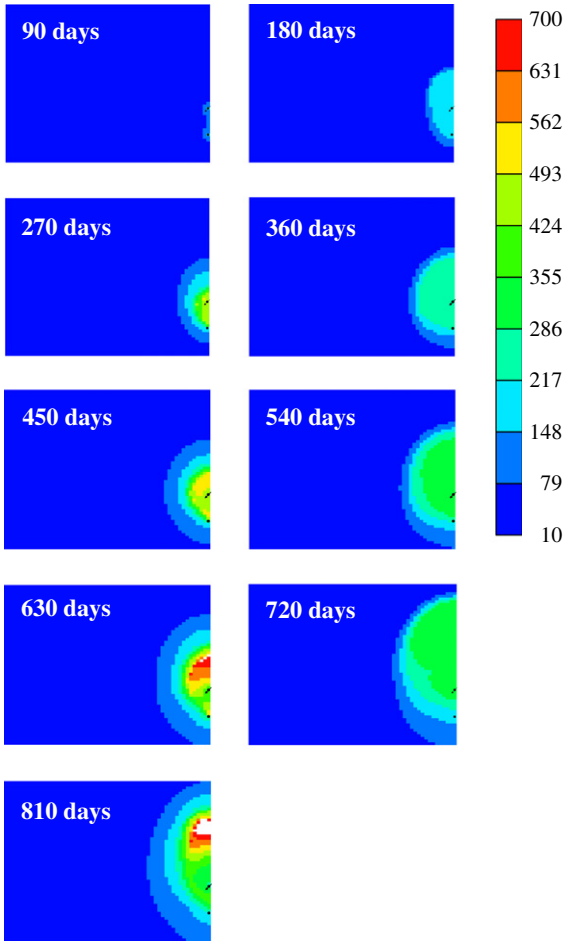

Fig. 14. Temperature (in °C) distributions at the end of each injection period (at end of oxygen injection period) during steam–oxygen cyclic injection process.

contribution to methane generation was not negligible. Given that hydrogen generation is higher than carbon monoxide, HMWG, and H_2S, the extent of coke gasification followed by the water–gas shift reaction were the main contributors to hydrogen generation which increased in later cycles. This observation is consistent with the existing literature [8]. The results show that despite lower oil production of the steam–oxygen ISG process, additional fuel in the form of mixture of H_2, CH_4, CO, CO_2, and other hydrocarbons, is generated during the process.

3.2. Energy intensity, emission to atmosphere and water usage

To compare total energy invested per total energy produced for the ISG process versus that for a conventional thermal oil sands recovery process, enthalpies of each input and output stream were calculated. It was found that the total energy produced was 7.4 $GJ_{(OUT)}$ (output energy in produced bitumen and fuel gas) per $GJ_{(IN)}$ (input energy in injected oxygen and steam including gas compression energy requirements) of energy injected during the ISG process. For a conventional thermal oil sands recovery process (SAGD), this ratio was equal to 6.9 $GJ_{(OUT)}$ (output energy in produced bitumen) per $GJ_{(IN)}$ (input energy measured in injected steam) of energy injected (this corresponds to a steam-to-oil ratio equal to about 2.3 m^3 per m^3). Thus, the energy output intensity from the ISG process was slightly greater than that of the SAGD process. Given that the produced energy vector now also consists of synthesis gas which does not require upgrading (natural gas requirement for upgrading is around 72 Sm^3 of natural gas per Sm^3 of bitumen processed [3,6] whereas CO_2 emission is around 6–17 kg per GJ SCO [34]), the overall energy intensity of the process taking upgrading of the bitumen into account is reduced. However, as shown in Fig. 13, the water usage in the steam–oxygen process was roughly one-half that of the SAGD process. These results are consistent with literature [24].

For the steam–oxygen ISG process, the CO_2 emission intensity (CO_2 emitted to surface per unit energy produced) was calculated to be 11.5 kg of CO_2 per GJ of energy produced (CO_2 emitted

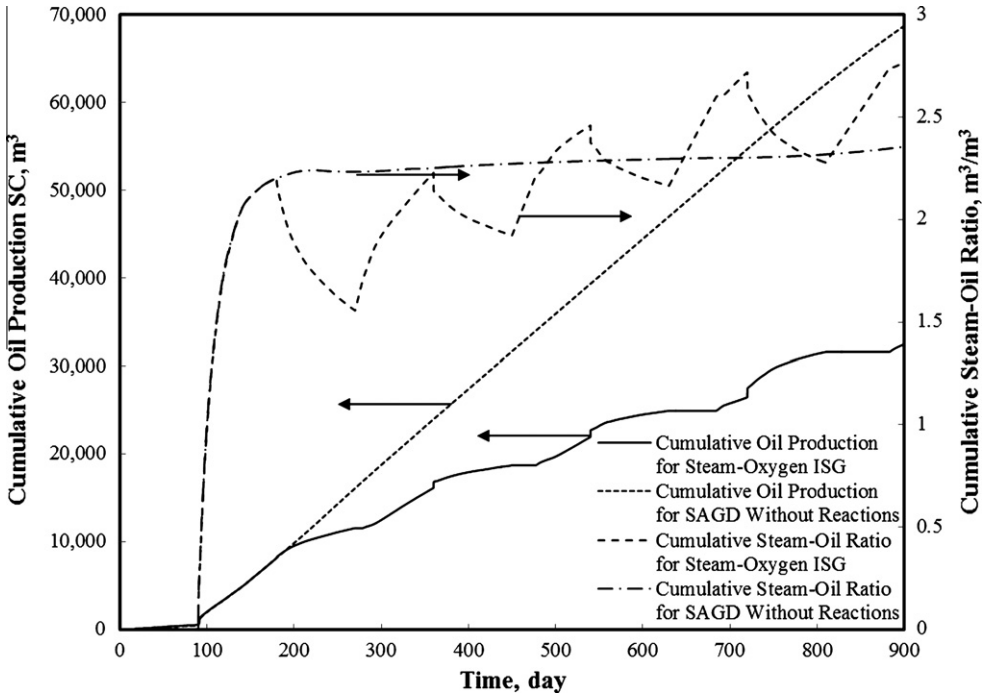

Fig. 15. Comparison of cumulative oil (at standard conditions) and cumulative steam–oil ratio for SAGD and steam–oxygen injection processes.

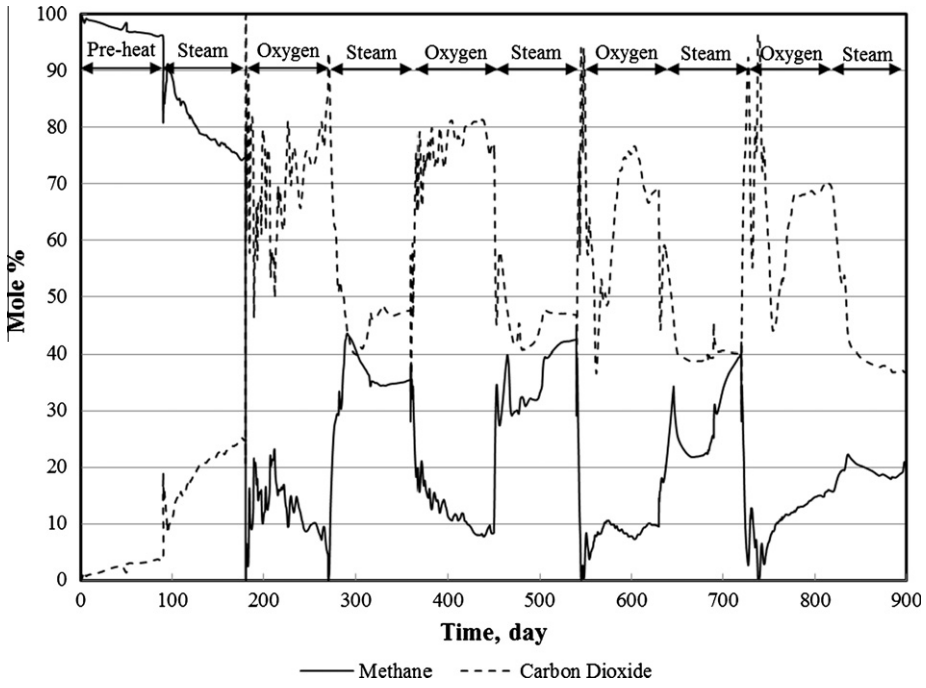

Fig. 16. Methane and carbon dioxide composition in produced gas from lower production well during cyclic injection of steam and oxygen.

includes that associated with energy consumed for gas compression, assuming 500 g CO_2 emitted per kW h of electricity [35], for injection and the amount in produced gases). This CO_2 emission for in situ bitumen gasification was slightly less than that of SAGD which emits 12.0 kg of CO_2 per GJ of energy produced.

In general, during steam injection, as it is conventionally done, the main product is bitumen along with small amounts of fuel and acid gases sourced mainly from solution gas and aquathermolysis reactions [36,37]. Injecting oxygen along with steam produces not only bitumen with comparatively lower greenhouse gas emissions, reduced water usage and higher energy efficiency, but also improved product mix from the reservoir including H_2, CO, CH_4, and higher molecular weight fuel gases. By varying the operating strategy through modulation of steam and oxygen injection rates and periods, the bitumen gasification process can be tuned to maximize fuel gas production.

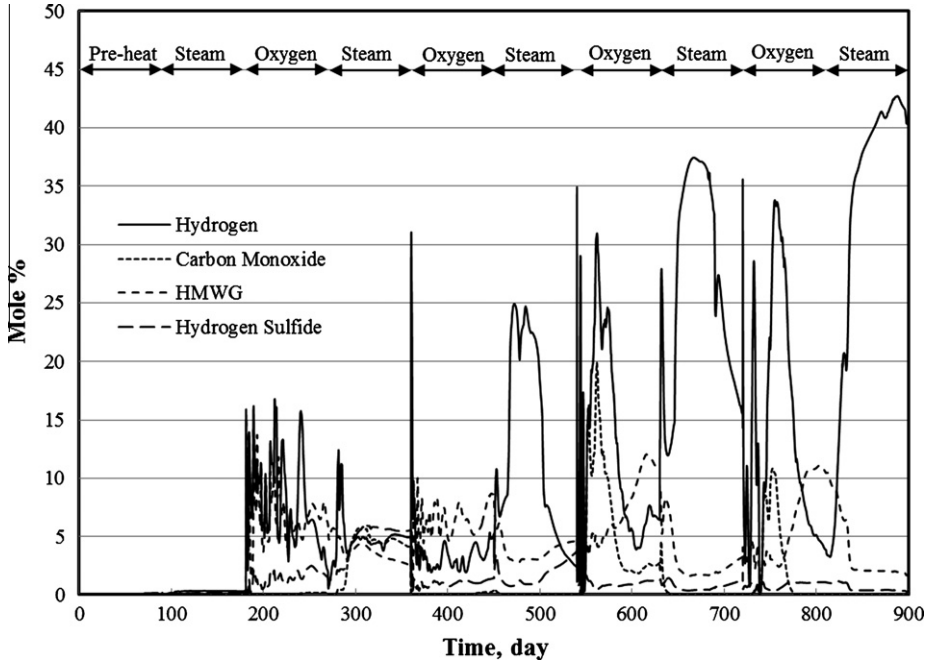

Fig. 17. Hydrogen, carbon monoxide, heavy molecular weight gas (HMWG), and hydrogen sulfide composition in produced gas from lower production well during cyclic injection of steam and oxygen.

The results from this study suggest that to design in situ bitumen gasification processes to maximize hydrogen production, the following points should be taken into account.

- Hydrogen production is maximum where there is the least amount of oxygen present (since ISC used to reach temperatures high enough to achieve gasification), so strategic placement of the producer well with respect to the injection well can maximize hydrogen production. In general, this means that the recovery process must be designed to avoid commingling of hydrogen and oxygen within the reservoir.
- Intermittent injection of oxygen, instead of continuous oxygen injection, can increase hydrogen production. This is similar to cyclic steam and air injection used for in situ coal gasification processes [39–41]. When oxygen is injected, the temperature in the combustion zone increases and after oxygen injection stops, the oxygen is consumed. Any generated hydrogen in this period may also be consumed. Directly following the combustion period, since temperatures are elevated, hydrogen-generating reactions continue and during this period large amounts of hydrogen can be produced from the system. After some time, the temperature will decline to the injected steam temperature and hydrogen generation will degrade. Based on economic considerations, air injection can resume to again raise the temperature in the system.
- The timing of air and steam injection periods must be optimized to maximize the target products from the reservoir. Under steam-only injection, bitumen is the largest product from the reservoir. Under steam–air injection, hydrogen and other fuel gases and bitumen are products from the process.

4. Conclusions

A comprehensive reaction scheme for ISC and gasification of bitumen has been developed for field scale modeling of ISG processes. This reaction scheme was matched against the Marguerite Lake ISC field pilot. Further the reaction scheme was used to predict hydrogen generation during ISG of bitumen for a recovery process with a SAGD well configuration. The results indicate that the hydrogen content in the produced syngas was as high as 20–30 mole percent consistent with results from the field data. In addition to hydrogen, other fuel gases such as methane and higher molecular weight fuel gases were produced. Also, the amount of energy produced per unit amount of energy invested for in situ gasification process was better than that for conventional recovery processes with less than half the water usage. Thus, with respect to water consumption, ISG process offer potential benefits. In terms of CO_2 emission to atmosphere, per unit amount of energy produced, bitumen gasification demonstrated slightly better results. Hence ISG processes for oil sands reservoirs will require optimization of the energy mix, whether oil, hydrogen, or fuel gases are produced. Additionally, these processes could potentially produce slightly upgraded oil (because of higher temperatures involved as compared to typical SAGD operations).

Acknowledgements

The authors acknowledge the financial support from the Alberta Ingenuity Center for In Situ Energy (AICISE), the Natural Sciences and Engineering Research Council (NSERC) of Canada, and a Zandmer Grant awarded by the Department of Chemical and Petroleum Engineering at the University of Calgary.

References

[1] Roadifer RE. Size distributions of the world's largest known oil and tar accumulations. In: Meyer RF, editor. Exploration for heavy crude oil and natural bitumen. American Association of Petroleum Geologist; 1987. p. 3–23.
[2] Meyer RF, Attanasi ED, Freeman PA. Heavy oil and natural bitumen resources in geological basins of the world. US Geological Survey; 2007. Report No.: 2007-1084.
[3] Energy Resources Conservation Board. Alberta's energy reserves 2010 and supply/demand outlook 2011–2020. ST98-2011; 2011.
[4] Central Intelligence Agency. The world factbook; 2011 January.
[5] Rosenfeld J, Pont J, Law K, Hirshfeld D, Kolb J. Comparison of North American and imported crude oil lifecycle GHG emissions. Prepared for Alberta Energy Research Institute. TIAX Case # D5595; 2009 July.
[6] Alberta Chamber of Resources. Oil sands technology roadmap, unlocking the potential; 2004 January.
[7] Guntermann K, Gudenau HW, Mohtadi M. Mathematical modeling of the in situ coal gasification process. In: Proceedings of the eighth underground coal conversion symposium; 1982 August. p. 297–306.

[8] Hajdo LE, Hallam RJ, Vorndran LDL. Hydrogen generation during in-situ combustion. In: Presented at the SPE California regional meeting. Bakersfield, California. SPE 13661; 1985 March 27–29.
[9] Babushok VI, Dakdancha AN. Global kinetic parameters for high-temperature gas-phase reactions. Combust Explos Shock Waves 1993;26(4):464–89.
[10] Belgrave JDM, Moore RG, Ursenbach MG, Bennion DW. A comprehensive approach to in-situ combustion modeling. SPE Advan Technol Ser 1993;1(1):98–107.
[11] Yang X, Gates ID. Combustion kinetics of Athabasca bitumen from 1D combustion tube experiments. Natur Resour Res 2009;18(3):193–211.
[12] Kapadia PR, Kallos MS, Gates ID. Potential for hydrogen generation from in situ combustion of Athabasca bitumen. Fuel 2011;90(6):2254–65.
[13] Kapadia PR, Kallos MS, Gates ID. A new kinetic model for pyrolysis of Athabasca bitumen. The Can J Chem Eng; in press. http://dx.doi.org/10.1002/cjce.21732.
[14] Donnelly JK, Hallam RJ, Duckett JA. An oil sands oxygen in situ combustion project. In: Proceedings of third UNITAR conference on heavy crude and tar sands. Long Beach, California, USA; 1985 July 22–31.
[15] Capeling RR. In-situ development at Marguerite Lake. In: Presented at Alberta oil sands technology and research authority's fourth annual advances in petroleum technology conference. Calgary, Alberta; 1983 May 30–31.
[16] Henningson CJ, Duckett JA. Oxygen fireflooding for in situ production of heavy oils and tar sands. In: Presented at fifth annual advances in petroleum recovery and upgrading technology conference. Calgary, Alberta; 1984 June 14–15.
[17] Hallam RJ, Hajdo LE, Staples S. Some operational aspects of the Marguerite Lake phase A oxygen in-situ combustion project. In: Heavy oil and tar sands production, upgrading and economics conference. Los Angles, California: PASHA Publications; 1985 December.
[18] Harding TG, Ejiogu GC. Pilot to commercial production of bitumen in the Wolf Lake area. In: Presented at advances in petroleum recovery and upgrading technology. Calgary, Alberta; 1986 June 12–13.
[19] Hallam RJ, Hajdo LE, Donnelly JK, Baron RP. Thermal recovery of bitumen at Wolf Lake. SPE Reser Eng 1989;4(2):178–86.
[20] Nzekwu BI, Hallam RJ, Williams GJJ. Interpretation of temperature observations from a cyclic-steam/in-situ-combustion project. SPE Reser Eng 1990;5(2):163–9.
[21] Hallam RJ. Operational techniques to improve the performance of in-situ combustion in heavy-oil and oil-sand reservoirs. In: Presented at the western regional meeting. Long Beach, California; 1991 March 20–22.
[22] Hallam RJ, Donnelly JK. Pressure-up blowdown combustion: a channeled reservoir recovery process. SPE Advan Technol Ser 1993;1(1):153–8.
[23] Kapadia PR, Wang J, Kallos MS, Gates ID. New thermal-reactive reservoir engineering model predicts hydrogen sulfide generation in steam assisted gravity drainage. J Petrol Sci Eng 2012;94–95:100–11.
[24] Yang X, Gates ID. Design of hybrid steam-in situ combustion bitumen recovery processes. Natur Resour Res 2009;18(3):213–33.
[25] Hayashitani M, Bennion DW, Donnelly JK, Moore RG. Thermal cracking of Athabasca bitumen. Oil Sands 1977;233–247.
[26] Adegbesan KO, Donnelly JK, Moore RG, Bennion DW. Liquid phase oxidation kinetics of oil sands bitumen: models for in situ combustion numerical simulators. AIChE J 1986;32(8):1242–52.
[27] Yasar M, Trauth DM, Klein MT. Asphaltene and resid pyrolysis. 2. The effect of reaction environment on pathways and selectivities. Energy & Fuels 2001;15(3):504–9.
[28] Martin WL, Alexander JD, Dew JN. Process variables of in situ combustion. Petrol Trans AIME 1958;213:28–35.
[29] Dingley AJ. The combustion recovery process principles and practices. In: Presented at the California regional meeting of the society of petroleum engineers of AIME. Bakersfield, California; 1965 November 4–5.
[30] Moore RG, Laureshen CJ, Belgrave JDM, Ursenbach MG, Mehta SA. In situ combustion in Canadian heavy oil reservoirs. Fuel 1995;74(8):1169–75.
[31] Moore RG, Laureshen CJ, Ursenbach MG, Mehta SA, Belgrave JDM. A Canadian perspective on in situ combustion. J Can Petrol Technol 1999;38(13).
[32] Information Handling Services. AccuMap user guide; 2011 November.
[33] Computer Modeling Group Ltd. STAR™ user's guide; 2011.
[34] Bergerson JA, Kofoworola O, Charpentier AD, Sleep S, MacLean HL. Life cycle greenhouse gas emissions of current oil sands technologies: surface mining and in situ applications. Environ Sci Technol 2012;46(14):7865–74.
[35] International Energy Agency. CO2 emissions from fuel combustion highlights. Edition 2011.
[36] Hyne JB. Aquathermolysis – a synopsis of work on the chemical reaction between water (steam) and heavy oil sands during simulated steam stimulation. Synopsis Report No. 50, AOSTRA Contracts No. 11, 103, 103B/C; 1986 April.
[37] Kapadia PR, Kallos MS, Gates ID. A new reaction model for aquathermolysis of Athabasca bitumen. Can J Chem Eng; 2012. doi:http://dx.doi.org/10.1002/cjce.21662.
[38] Green DW, Perry RH. Perry's chemical engineers' handbook. 8th ed. Berlin: McGraw-Hill; 2008.
[39] Terry RC. Method and apparatus for in situ gasification of coal and the commercial products derived therefrom. US Patent 3952802. Issued April 27th, 1976.
[40] Garret DE. Process for the gasification of coal in situ. US Patent 4087130.Issued May 2nd, 1978.
[41] Bhutto AE, Bazmi AA, Zahedi G. Underground coal gasification: from fundamentals to applications. Progr Energy Combust Sci 2013;39(1):189–214.